A 6-Wafer Combustion System for a Silicon Micro Gas Turbine Engine

Amit Mehra, Xin Zhang, Arturo Ayón, Ian Waitz, Martin Schmidt and Christopher Spadaccini

Abstract

As part of a program to develop a micro gas turbine engine capable of producing 10-50 Watts of electrical power in a package less than one cubic centimeter in volume, we present the design, fabrication, packaging and experimental test results for the 6-wafer combustion system for a silicon microengine. Comprising the main non-rotating functional components of the engine, the device described herein measures 2.1 cm × 2.1 cm × 0.38 cm, and is largely fabricated by deep reactive ion etching through a total thickness of 3,800 μm. Complete with a set of fuel plenums, pressure ports, fuel injectors, igniters, fluidic interconnects, and compressor and turbine static airfoils, this structure is the first demonstration of the complete hot flow path of a multi-level micro gas turbine engine. The 0.195 cm^3 combustion chamber is shown to sustain a stable hydrogen flame over a range of operating mass flows and fuel-air mixture ratios, and to produce exit gas temperatures in excess of 1600K. It also serves as the first experimental demonstration of stable hydrocarbon microcombustion within the structural constraints of silicon. Combined with longevity tests at elevated temperatures for tens of hours, these results demonstrate the viability of a silicon-based combustion system for micro heat engine applications.

Amit Mehra, Ian Waitz and Christopher Spadaccini are with the Gas Turbine Laboratory, Department of Aeronautics and Astronautics, Massachusetts Institute of Technology.

Xin Zhang, Arturo Ayón and Martin Schmidt are with the Microsystems Technology Laboratories, Department of Electrical Engineering and Computer Science, Massachusetts Institute of Technology.

Portions of this work were presented at the International Conference on Solid-State Sensors and Actuators, Sendai, Japan, 1999.

I. Introduction

RECENT advances in the field of silicon microfabrication technology have opened the potential for miniature combustion engines for portable power generation and micro air vehicle propulsion applications [1]. As part of a current Massachusetts Institute of Technology (MIT) program to develop such technologies, Epstein *et al.* [2] and Groshenry [3] have reported the design for a micro gas turbine generator capable of producing 10-50 Watts of electrical power while consuming 7 grams of jet fuel per hour.

A discussion of relevant combustor scaling laws and preliminary assessments of several combustor concepts for these applications were presented by Waitz *et al.*[4]. Stable hydrogen combustion in a microfabricated silicon combustor for this engine was first demonstrated by Mehra and Waitz [5], who showed that it was possible to attain exit gas temperatures in excess of 1800K without compromising the structural integrity of the 0.066 cm^3 combustion chamber. An SEM of this silicon microcombustor is shown in Figure 1, along with a schematic of the baseline engine configuration.

The device shown in Figure 1 served as the first demonstration of a high power density microcombustion system ($\sim$2000 MW/m^3, [6]); efforts were subsequently undertaken to integrate it with the rest of the engine.

This paper reports the results of those integration efforts by presenting the design, fabrication, packaging and experimental testing of the combustor in a typical *engine* configuration. Complete with fuel plenums and injection holes, pressure diagnostics, igniters, and compressor and turbine static airfoils, the resulting device is referred to as the "static structure", and serves as the first demonstration of the completed hot flow path of a multi-level micro gas turbine engine.

The paper is specifically intended to:

1. Describe the use of deep reactive ion etching and aligned fusion bonding to fabricate a 3,800 μm thick, 6-wafer level static structure for a microengine,

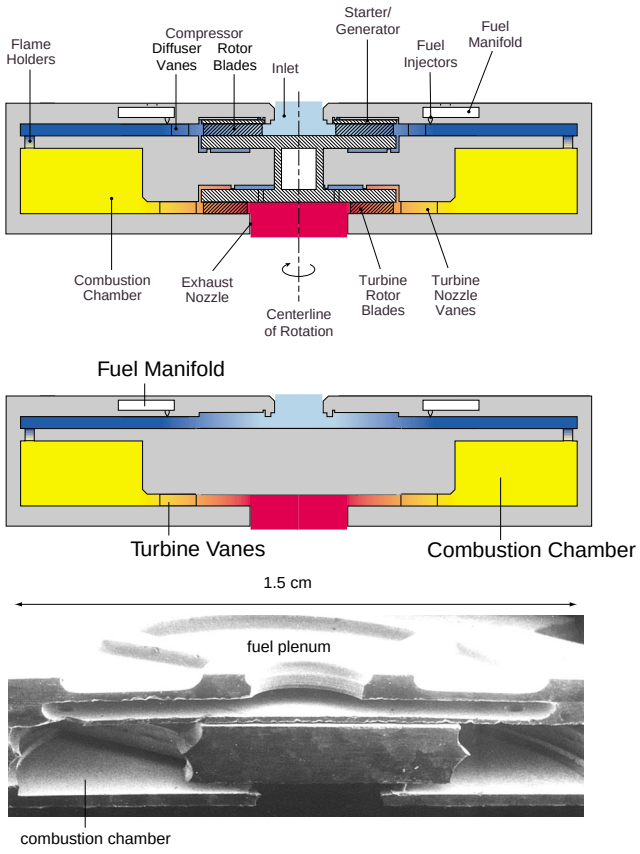

Fig. 1. Schematics of the baseline engine and combustor configurations, along with an SEM of the first silicon microcombustor.

2. Present a unique design that allows high temperature, high efficiency hydrogen microcombustion in the device over a range of fuel-air ratios, and with low overall heat loss, and

3. Present the first experimental demonstration of stable hydrocarbon microcombustion within the structural constraints of a silicon device.

Before describing the detailed design, fabrication and test results of the static structure however, we begin by presenting an overview of the challenges facing microcombustor design.

II. Microcombustor Design Issues

The ability to transfer the chemical energy of a fuel into a fluid at high mass flow rates and in small volumes makes the power density of a microcombustor particularly appealing for portable power generation and micropropulsion applications [6]. The realization of high power density however,

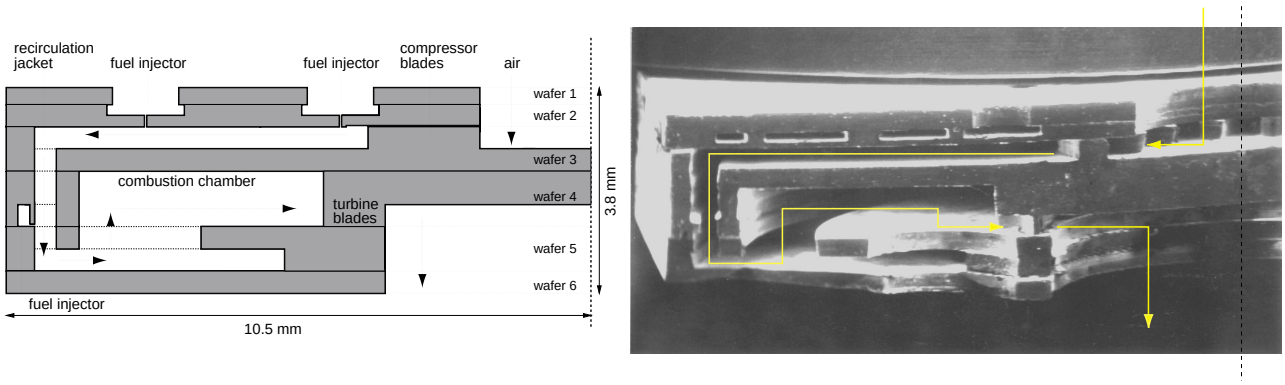

Fig. 2. Schematic and SEM cross-section of half of the axisymmetric 6-wafer static structure. (Note: The dies on the wafer had two types of combustor inlet holes - one type had slots as shown in Figure 3, the other had an annular opening as shown above.)

requires effective completion of the combustion process within a small volume, and is therefore fundamentally limited by the chemical reaction time constraints of the fuel. Tailoring the fluid flow to stabilize the flame and allow effective mixing of the cold reactants with the hot products is therefore critical to getting the fuel to completely react within a short time, and constitutes a fundamental design challenge.

This chemical kinetics constraint is also exacerbated by the enhanced heat transfer effects that result from the large surface area-to-volume ratio of these devices. Not only does this high heat loss make it impossible to achieve conventional combustor efficiencies in excess of 99.9%, it also increases chemical reaction times by lowering the temperature of the flame stabilization zones. The coupling between the fluid dynamics, heat transfer and chemical kinetics is therefore much more pronounced for these small systems, and is a critical element of the design process.

The design space is further complicated by the addition of a third factor - the material and fabrication constraints. While silicon microfabrication is instrumental to achieving the economy and high tolerances necessary to make a microengine viable, it is still largely limited to rudimentary 3-D geometries. Furthermore, while creep constraints in the rotating components limit wall temperatures to 900K [7], chemical kinetics demand higher temperatures to achieve stable and

efficient combustion. The walls of the combustor therefore have to be cooled below the operating gas temperatures inside the chamber. Since cooling the hot chamber walls can adversely impact the efficiency of the combustor, designing a device that is efficient, yet structurally durable, poses a significant design challenge.

The design of a microcombustor therefore mandates careful trade-offs between power output, thermodynamic cycle parameters associated with the engine, physical dimensions, and material and manufacturing capabilities. These design considerations are described in the following sections[1].

III. Design of the Static Structure

A schematic of the static structure is shown in Figure 2, alongside an SEM of the fully-bonded 6-wafer device. Detailed views of each of the wafers prior to bonding are also shown in Figure 3, along with an exploded 3-D schematic of the individual wafers. As highlighted on the pictures, air enters the device axially and makes a right angle turn into the compressor. In the absence of a spinning rotor, stationary compressor blades are used to provide the requisite flow angle into the combustor. Fuel is injected through a circular array of holes, and allowed to mix with the air as it flows through the combustor recirculation jacket. The flow then enters the combustor through an axial inlet, burns in the 0.195 cm^3 annular shaped volume, and finally exhausts through turbine static vanes that were designed to maintain an elevated operating pressure in the chamber by choking the flow. (In the engine, the flow would also pass through the spinning turbine rotor for power extraction prior to being exhausted out of the engine.)

The volume of the combustion chamber in the static structure was determined by re-scaling the volume of the 3-stack microcombustor, which operated at atmopheric pressure, in order to obtain the same residence time at the design operating conditions of the 6-stack [5]. The maximum die

[1]The design and operation of such microsystems is also complicated by the difficulty in instrumenting the small experimental rigs. The inapplicability of conventional diagnostics mandates the development of "on-chip" sensors for temperature, pressure, etc.; efforts are currently underway to incorporate these transducers in future devices.

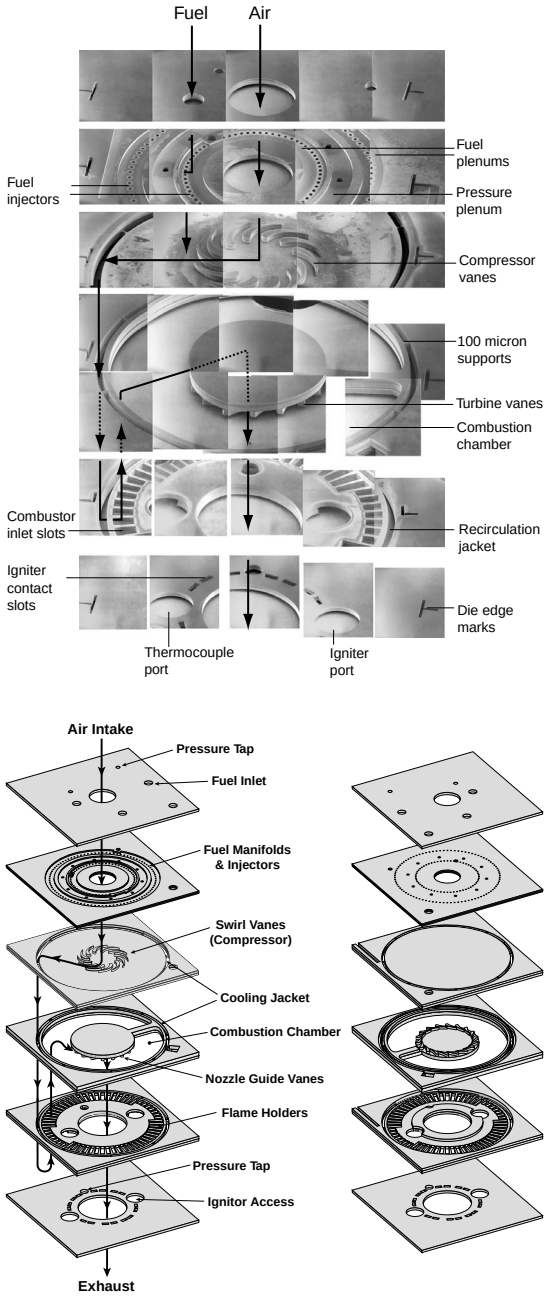

Fig. 3. A composite of 35 SEM's of the individual wafers prior to bonding along with an exploded schematic showing the detailed fluid flow path. (Note: This die has slotted openings into the combustion chamber.)

size was also limited to 2.1 cm to accommodate at least ten dies on a 4" wafer. Table I shows the design operating parameters for the static structure, and compares them with those for the previously demonstrated 3-stack microcombustor.

	3-stack	Static structure
Air flow rate	0.18 gm/sec	0.36 gm/sec
Operating pressure	4 atm.	3 atm.
Overall die size	15 × 15 × 1.8	21 × 21 × 3.8 mm
Combustor o.d.	10 mm	18.4 mm
Combustor i.d.	5 mm	9.6 mm
Combustor height	1 mm	1 mm
Combustor volume	66 mm^3	190 mm^3
Residence time	0.5 msec	0.5 msec

TABLE I

Operating parameters for the 3-stack microcombustor and the static structure. (Note: The flow residence times are based on an average flow temperature of 1000K.)

A. Design of the Recirculation Jacket

Previous experimental testing of the 3-stack microcombustor had shown that although ambient heat loss from the structure reduced the combustor efficiency to approximately 70%, it was instrumental to the survival of the silicon; the walls of the combustion chamber operated at hundreds of Kelvin below the combustor gas temperature [5]. In an attempt to improve combustor efficiency without violating the structural integrity of the device, the static structure incorporated a combustor recirculation jacket as shown in Figure 2. The recirculation jacket was designed to:

1. Recover the lost energy of the combustion chamber to pre-heat the incoming reactants, while
2. Allowing the compressor discharge air to cool the hot walls of the chamber, enabling the silicon to survive at the high gas temperatures needed for stable combustion.

Using computational fluid dynamics (CFD) solutions[2], the size of the recirculation jacket was set at a maximum possible width of 400 μm to minimize the pressure loss within the duct. In order to support the interior chamber, eight 100 μm wide bridges were used to connect it with the outer walls. These bridges were also intended to minimize the heat conduction between the combustion chamber and the outer walls of the device. Pictures of these features are shown in Figure 4.

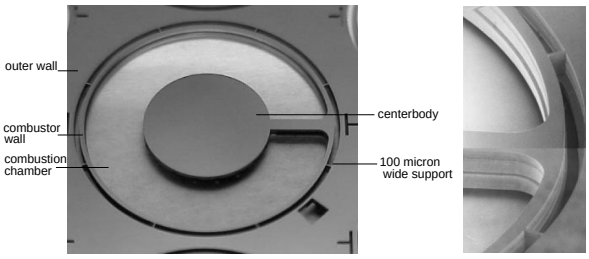

Fig. 4. Pictures of the eight 100 μm bridges that connected the combustion chamber to the outer walls of the static structure.

B. Fuel Injector Design

As shown in Figure 2, the static structure was designed with three sets of fuel injectors located at different points along the flow path to evaluate the trade-off between mixing effectiveness and potential upstream burning in the recirculation jacket. The size and spacing of the injector holes was determined by using semi-empirical models to optimize the penetration and lateral spreading of the jets in order to minimize the streamwise length needed for complete fuel-air mixing [9]. Four of the six dies on the wafer were optimized for hydrogen injection; the remaining six were intended for propane. The final design resulted in two sets of axial arrays located downstream of the compressor vanes at a radius of 4.8 mm and 8 mm respectively, and one set of radial fuel injectors located at the base of the recirculation jacket. Their number and diameters ranged from 60-90, and 120-224 μm, respectively. A picture of these injectors is shown in Figure 5.

[2]These calculations were performed using Fluent v. 4.2. Details of the application of this code can be found in Reference [8].

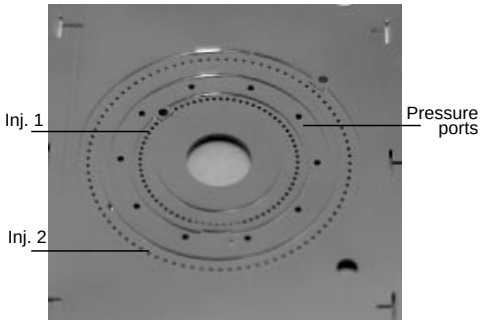

Fig. 5. Image of the fuel plenums and axial fuel injectors in the static structure.

C. Design of the Flame Holders

Since residence time constraints limited the completion of the chemical reactions inside the combustion chamber, a combination of CFD and chemical kinetic models were used to tailor the flame stabilization and flow recirculation zones inside the chamber. The objective of this exercise was to maximize the range of mass flows and heat loss conditions over which a stable flame could be sustained in the combustion chamber while at the same time maximizing the combustor efficiency. Recirculation zones are reservoirs for hot products and serve as the ignition source for the reactants flowing into the combustor. The size and shape of the recirculation zones within the combustor are set in part by the combustor inlet geometry. In designing the recirculation zones, one desires them to be large enough to serve as effective ignition and flame stabilization sources, but not so large as to take up most of the conbustor volume, thereby reducing the residence time for the reactants and negatively impacting the combustor efficiency. Further, the temperature of the recirculation zones is a function of their size and shape, being set by interfacial exchange and mixing as well as heat loss at the wall.

Two different designs were tested:

1. The first configuration was composed of sixty slots that were 2.2 mm long, and had an inner and outer radius of 7 mm and 9.2 mm, respectively, and produced many small recirculation zones at the entrance of the combustor. These would tend to increase combustor efficiency at the expense

of stable operating range.

2. The second configuration was a single annular opening that was 1.2 mm wide producing a single large recirculation zone within the combustor. This configuration would be expected to allow operation over a wide range of conditions, but with poorer combustor efficiency.

SEM's of both these configurations are shown in Figure 6.

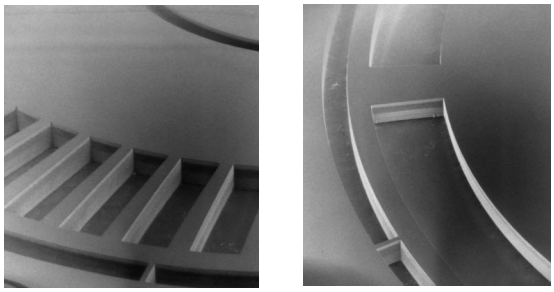

(a) Slotted inlet. (b) Annular inlet.

Fig. 6. SEM's of the two combustor inlet configurations. (Note: The 100 μm wide supporting bridges can also be seen in the images. The slots are 2.2 mm long; the annulus is 1.2 mm wide.)

IV. Fabrication Process

The fabrication of the static structure required ten deep dry anisotropic etches and two shallow etches. A total of thirteen masks were required for the process, including one global alignment mask. The steps are illustrated in Figure 7, the process is listed as follows:

A. Photolithography and Deep Reactive Ion Etching

Wafer 1 required a single 400 μm deep dry anisotropic etch to define the inlet holes to the three fuel plenums, the pressure plenum, and the compressor.

Wafer 2 was first 5 μm shallow etched from the bottom to define the tip clearance for the compressor. (Even though there were no rotating blades in the static structure, the clearance was required to maintain the thermal insulation between the combustion chamber and the outer walls

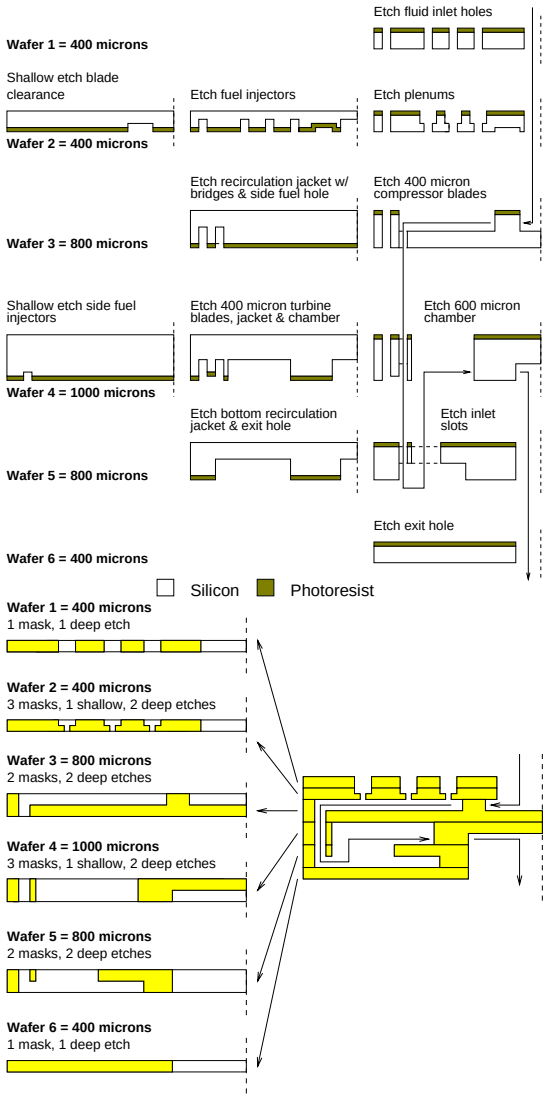

Fig. 7. An illustration of the fabrication process for the 6-wafer static structure, along with a schematic cross-section of each of the wafers prior to bonding. (Note: The cross-sections are not to scale.)

of the device.) Following the shallow etch, the wafer was flipped and 200 μm deep fuel and pressure plenums were anisotropically dry etched from the top. Finally, 200 μm deep axial fuel injector holes were anisotropically dry etched from the bottom.

Wafer 3 comprised the inflow swirl vanes and involved two 400 μm deep anisotropic etches. The 400 μm compressor blades were first etched from the top side, the wafer was then flipped, and finally, the 400 μm recirculation jacket was etched from the bottom.

Wafer 4 comprised the 1000 μm deep combustion chamber and the turbine NGV's. First, 5 μm

deep radial fuel injectors were etched on the bottom surface of the wafer. The 400 μm deep NGV blades were then etched from the bottom. Finally, the wafer was flipped, and the remaining 600 μm of the combustion chamber was etched from the top.

Wafer 5 contained the combustor inlet holes, and like wafer 3, also involved two 400 μm deep anisotropic etches. The combustor inlet slots were first etched on the top side of the wafer. The remaining 400 μm of the recirculation jacket was then etched from the bottom.

Wafer 6 required a single 400 μm etch for the exit hole, the igniter ports, and the aft pressure port.

For each of the patterning steps, 10 μm of positive photoresist was used as a mask (Hoechst AZ 4620); the wafers were patterned using double-sided infra-red alignment. The deep etches utilized a time-multiplexed inductively-coupled plasma of SF_6 etchant and C_4F_8 passivating polymer. The performance of the etcher was optimized by characterizing the recipes over a wide parameter space [10], thereby allowing the fabrication of high tolerance and high aspect ratio structures such as the 400 μm high compressor and turbine airfoils, and a 1000 μm deep combustion chamber supported by 100 μm wide bridges.

Figure 8 shows pictures of the device along different axial planes.

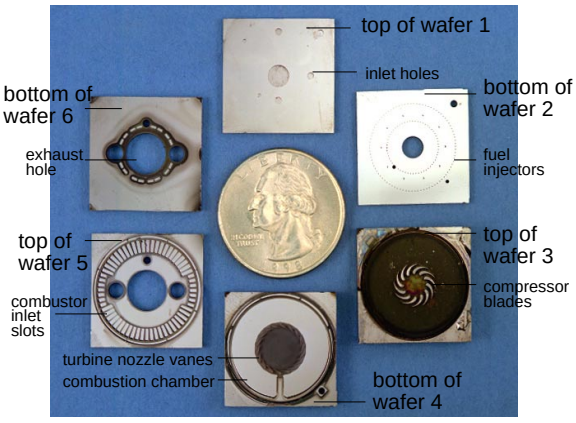

Fig. 8. Die-level image of the different layers in the 6-wafer static structure. (Picture courtesy: MIT Lincoln Laboratory)

B. Aligned Fusion Bonding

Following the completion of individual processing, the wafers were aligned fusion bonded. The wafers were RCA-cleaned first [11], then aligned bonded, and finally post-annealed in an 1100°C furnace for one hour.

Given the complexity of bonding six patterned wafers with thicknesses varying between 400 μm and 1000 μm, and a total stack thickness of 3,800 μm, this step posed a significant challenge. In fact, the first two builds of the static structure suffered from poor bonding yield, and produced dies that leaked along the bondlines upon pressurization.

This low bonding yield was traced to surface contamination resulting from passivating fluorocarbon deposits on the bottom surface of the wafers during through-wafer DRIE. Subsequently, sacrificial oxide coatings were used to protect the back side of all wafers during through-wafer etches. The bonding protocol was also improved to minimize wafer handling, and to allow multiple wafer bonding of all six wafers in one single step.

As a result of these measures, wafer bonding on the final build produced 100% yield at diesaw; an infra-red image of this bonded stack is shown in Figure 9.

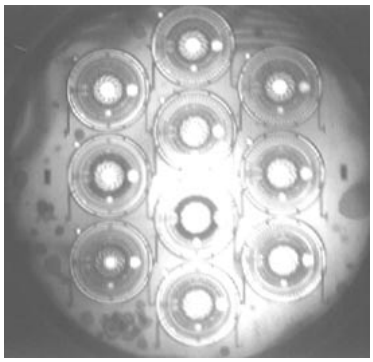

Fig. 9. Infra-red image of the six wafer stack showing good bond quality over most of the wafer.

V. Packaging

Packaging the static structure in an experimental test rig required:

1. Five front side fluidic connections for main air, three fuel lines, and one upstream pressure port.
2. One back side fluidic connection for the aft pressure port in the combustion chamber.
3. One backside electrical connection for the igniter.

The requirement for pressure-sealed electrical and mechanical interconnects was complicated by the high temperature operating environment of the device. (The walls were expected to operate at temperatures of approximately 1000K; the device was intended to be tested at pressures as high as 5 atm.)

After initial attempts with high temperature ceramic adhesives, fluidic interconnects for the static structure were made via a glass bead interconnect scheme developed by London, Harrison and Spearing for similar applications in a micro rocket engine [12]. As illustrated in Figure 10, this interconnect was made by heating an annular-shaped glass-preform in a 1300K furnace to directly bond a kovar tube to the silicon surface.

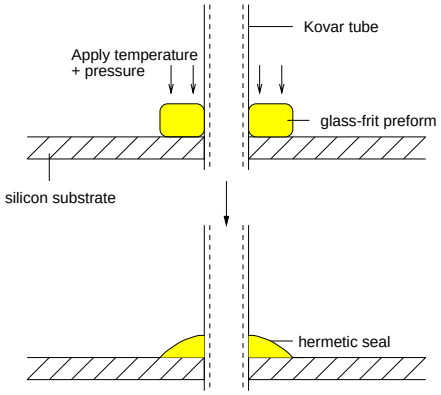

Fig. 10. An illustration of the process used to make the glass bead interconnects to the static structure.

An electrical igniter was also similarly packaged by potting a kovar wire in glass and pressure sealing the fixture through the back side of the static structure. The wire was then resistively heated to ignite the fuel-air mixture and initiate combustion inside the chamber.

Figure 11 shows pictures of the static structure in its final configuration. (The braze plate at the other end of the kovar tubes was directly attached to a macrofabricated fixture with conventional

o-ring fittings.)

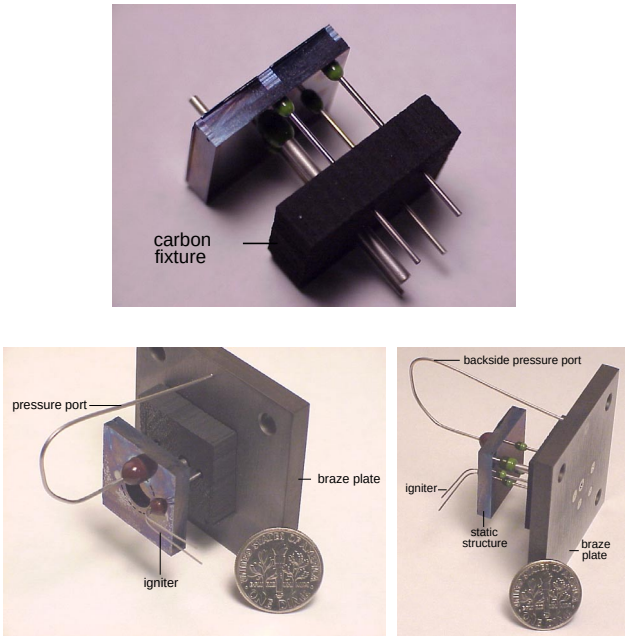

Fig. 11. Pictures of the fully-packaged static structure with mechanical and electrical igniter interconnects. (Note: The carbon fixture was used to align the kovar tubes.)

VI. Experimental Test Results

Following satisfactory packaging of the device, the static structure was experimentally tested with the following instrumentation:

1. Mass flow controllers to monitor the fuel and air mass flow rates.

2. Two type K, 0.010" sheathed thermocouples to measure the temperature of the outer walls.

3. One type K, 0.010" sheathed thermocouple to measure exhaust gas temperature at the exit.

4. Digital pressure transducers to measure the static pressure in the upstream recirculation jacket and inside the combustion chamber.

A. Effectiveness of the Recirculation Jacket

In order to compare the performance of the static structure with that of the previously demonstrated 3-stack microcombustor [5], premixed hydrogen-air combustion tests were carried out in

the static structure at the atmospheric design mass flow rate of the 3-stack microcombustor ($\dot{m}_a$=0.045 g/sec). These tests were intended to compare the two devices under back-to-back test conditions, and allow quantification of any performance increase that might result due to the presence of the recirculation jacket, or from improved packaging schemes.

Figure 12 compares the experimentally measured exit and wall temperatures for the two devices under similar operating conditions. The plot shows an increase in static structure exit gas temperature and a corresponding decrease in outer wall temperature. It also suggests that the static structure is capable of attaining the desired 1600K turbine inlet temperature at a lower equivalence ratio - this results in a lower fuel consumption that is reflected in an increased efficiency as shown in Figure 13.

The presence of the recirculation jacket and a larger combustion chamber therefore improves the efficiency of the combustor by 15-50% over the previously described 3-stack. The outer wall temperatures are also lower by approximately 100K, reducing the overall heat loss, and making packaging of the device somewhat easier.

Overall, these tests demonstrate the feasibility of high temperature, high efficiency microcombustion within the structural constraints of a silicon combustor, and with low overall heat loss from the device.

B. Hydrogen Combustion Tests

Additional hydrogen-air tests were subsequently conducted inside the static structure in order to characterize the operating space for hydrogen-air combustion. Figures 14 and 15 plot the exit gas temperatures and combustor efficiency as a function of mass flow rate for different fuel-air ratios. The corresponding outer wall temperature under these conditions is plotted in Figure 16. The figures show exit gas temperatures in excess of 1600K, and overall efficiencies as high as 95%. The operating temperature of the outer wall is also seen to be limited below 750K due to the insulating

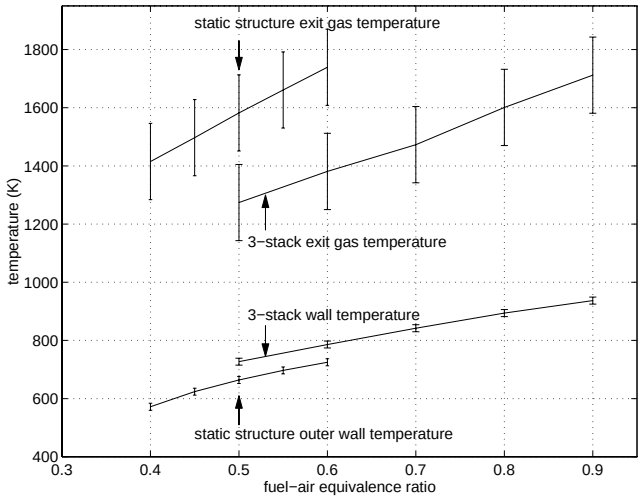

Fig. 12. Exit and wall temperature measurements, showing an increase in the static structure exit temperature, and a decrease in outer wall temperatures.

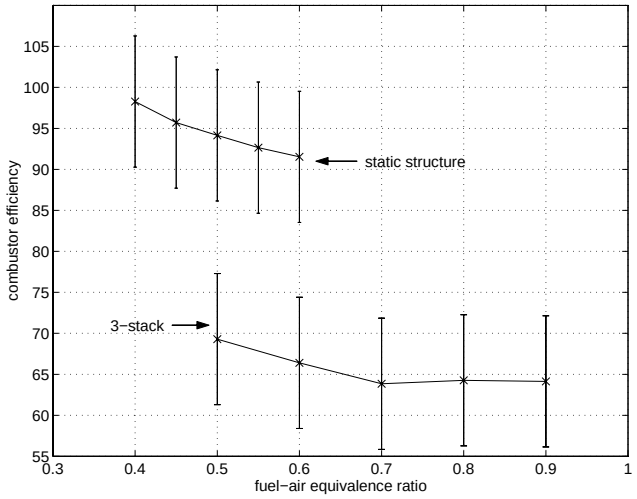

Fig. 13. Efficiency measurements in the static structure and 3-stack microcombustor.

properties of the combustor recirculation jacket.

Stable combustion could only be sustained up to approximately one-third of the design mass flow rate of the device. The device was designed to operate with choked turbine vanes and thus elevated pressures in the combustion chamber. However, it was found during testing that the minimum ratio of residence time to chemical kinetic time did not occur at the design point but rather in the unchoked portion of the operating regime ($\dot{m}$ less than approximately 0.2 g/s). This led to blow out prior to the attainment of the high operating pressures needed to sustain stable combustion

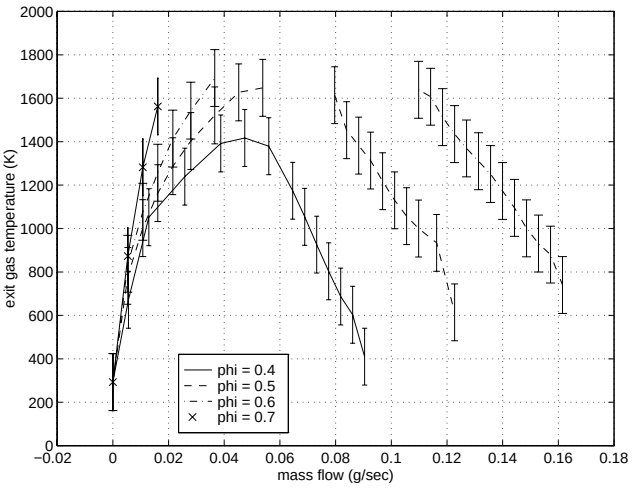

Fig. 14. Exit temperature measurements in the static structure as a function of mass flow rate for different fuel-air equivalence ratios. (Note: The break in the ϕ=0.5, 0.6 curves results form the inability to measure exit gas temperatures in excess of 1600K; the ϕ=0.7 curve stops at a mass flow rate of 0.015 gm/sec due to initiation of upstream combustion in the recirculation jacket at low mass flow rates and high fuel-air mixture ratios.)

inside the device at design mass flow rates. For ϕ=0.6 at a mass flow rate of 0.16 g/s, the residence time in the combustor was approximately 0.65 ms. The minimum residence time at which a flame was stabilized in the device was approximately 0.42 ms.

A closer examination of the heat transfer through the device also showed that at low mass flow rates, the heat loss to the ambient constituted a significant fraction of total heat generated inside the chamber. Along the left-hand side of the curves in Figures 14 and 15, the performance of the combustor was therefore limited by the low *thermal* efficiency of the device.

As the mass flow rate of the device was increased along a constant equivalence ratio curve, the heat loss became a small fraction of the total heat generated (approximately 5 Watts out of 100). The thermal efficiency of the device therefore approached unity at high mass flow rates, however, decreasing residence time limited the *chemical conversion* efficiency in this regime. Along the right-hand side of the curves in Figures 14 and 15, the performance of the combustor was therefore limited by the low *chemical* efficiency of the device. Further discussion of the analysis that supports

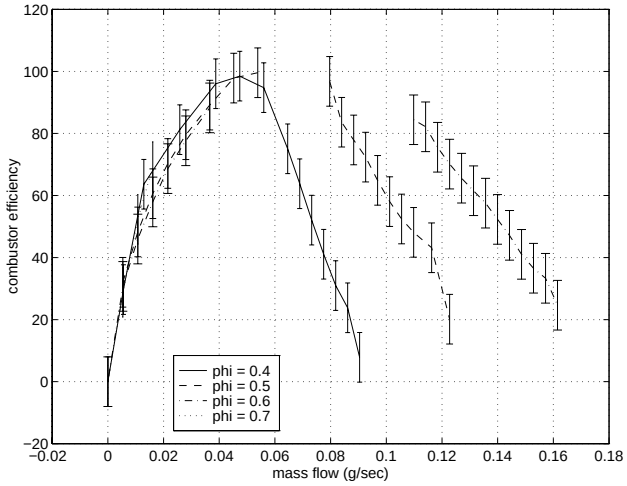

Fig. 15. Efficiency measurements in the static structure.

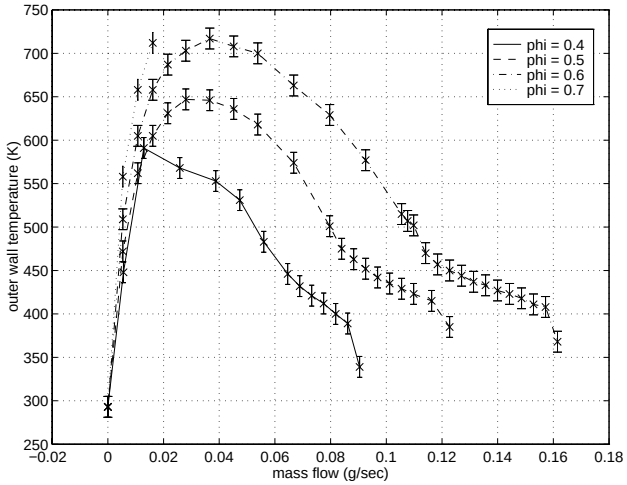

Fig. 16. Outer wall temperature measurements.

these assertions is contained in Mehra [8].

Efforts are currently underway to extend the blow out boundaries of the device by independently controlling the pressure-mass flow characteristic of the device in order to increase the operating pressure inside the chamber.

Among the two different inlet geometries, the slotted inlet configuration was found to exhibit significantly higher efficiency near (95% for 0.044 g/s $< \dot{m} <$ 0.12 g/s) for the kinetically-limited regime of the operating space. This was attributed to the presence of multiple, small recirculation

zones between the slots; these were more effective in facilitating uniform and rapid ignition of the incoming reactants, thereby increasing the chemical conversion efficiency of the device at high mass flow rates. As expected, the smaller recirculation zones were also less stable resulting in quenching of the reaction at lower mass flow rates. The maximum stable operating range of the device was 10% lower than for the annular inlet geometry.

C. Fuel Injection Tests

In addition to premixed hydrogen-air combustion tests, non-premixed tests were also conducted to evaluate the performance of the three fuel injection schemes. Figure 17 plots the exit gas temperature and efficiency measurements for the three different fuel injection schemes and compares them with results from the premixed tests. The figure shows a 5-point drop in efficiency due to fuel-air unmixedness upon injection through the first set of axial injectors; injection further downstream has up to a 50-point impact on efficiency.

Injection through the first set of radially located holes is therefore considered to be acceptable; the mixing is expected to improve further as the injectors are operated closer to design conditions. Efforts are currently underway to do additional testing in order to evaluate the performance of the injectors at higher mass flow rates and pressures[3].

D. Materials and Structural Tests

The static structure was tested at high temperatures and pressures for several hours. Figure 18 plots the cold flow curves for one of the devices after up to 38 hours of combustion testing. (The gas temperatures during these tests exceeded 1800K.) The curves show minimal change, suggesting that the device continues to pressure seal after high temperature operation. The ultimate failure

[3] A potential negative effect of injecting fuel through the first fuel injector configuration lies in the possibility of initiating combustion in the upstream recirculation jacket. However, since upstream combustion was only observed at very low mass flow rates, it is not expected to be a concern in the high mass flow, design-operating regime of the microengine.

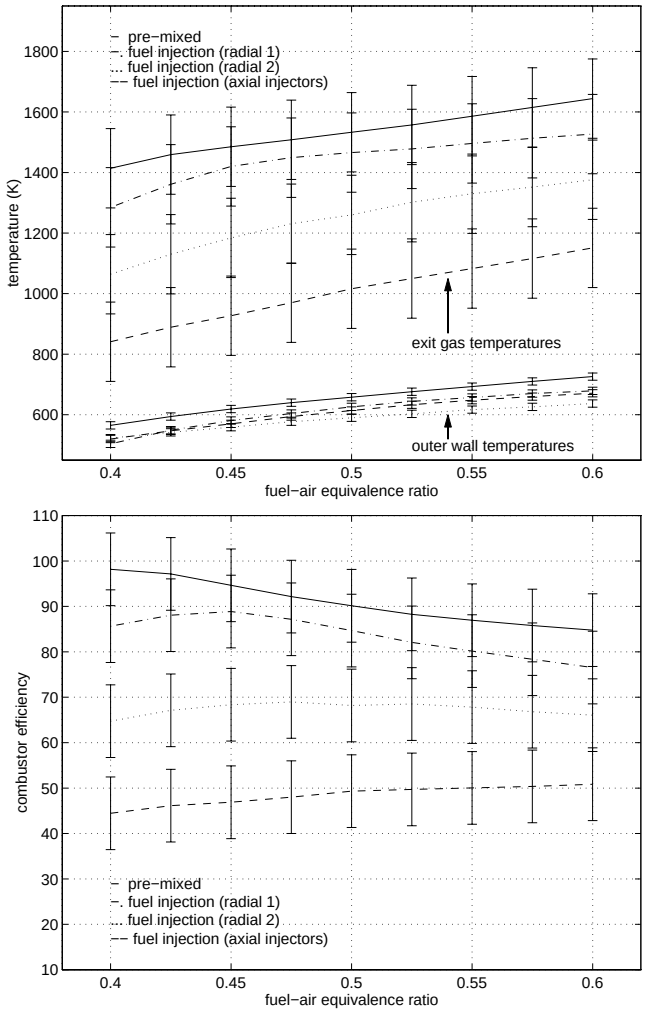

Fig. 17. Comparison of the temperature and efficiency measurements for the three non-premixed injection schemes with those from the premixed case, showing acceptable performance for injection through the first set of axial injectors.

resulted from silicon fracture due to initiation of the combustion in the recirculation jacket.

These results therefore demonstrate the structural integrity of the device at high temperatures, and pressures up to 1.3 atm, so long as the mixture does not burn in the upstream recirculation jacket. Efforts are currently underway to evaluate the structural integrity of the device at higher pressures and mass flow rates.

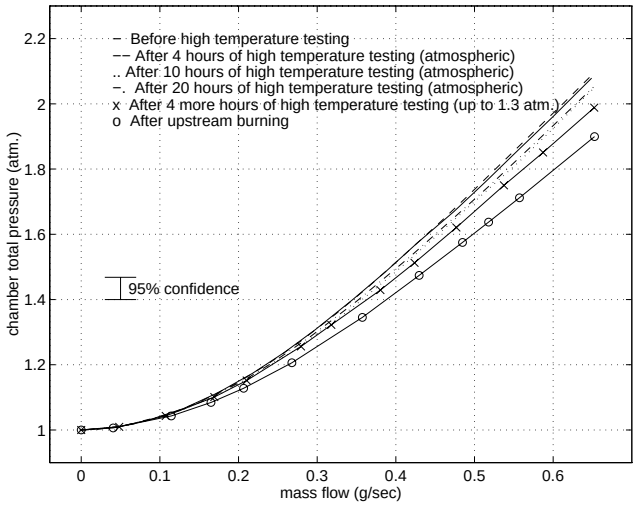

Fig. 18. Cold flow curves for the static structure after progressive high temperature exposure.

E. Hydrocarbon Test Results

Although the fast chemical reaction rates of hydrogen allow it to serve as an ideal fuel for a residence time limited microengine, storage and increased energy density requirements ultimately dictate the use of a hydrocarbon fuel for micro air vehicle propulsion and portable power applications. Tests were therefore also carried out to identify the stable operating regime for hydrocarbon combustion in the static structure.

Based on the ratio of the laminar flame speed for hydrogen-air and hydrocarbon-air combustion, the reaction rate for hydrocarbon fuels can be expected to be slower than that for hydrogen by a factor of 5-50 [13] & [14]. This suggests the need for a larger combustion chamber for design point hydrocarbon operation in the microengine. Alternatively, for a given volume, hydrocarbon combustion may be stabilized at lower mass flow rates, (and hence power densities).

Figures 19 and 20 plot the experimentally measured exit gas temperatures for ethylene-air and propane-air combustion in the static structure[4]. To date, these tests have demonstrated stable ethylene-air combustion with exit gas temperatures in excess of 1600K, combustor efficiencies be-

[4]The reaction rates for ethylene are approximately twice as high as those for propane [14], hence, it was considered more favorable from a chemical kinetics perspective.

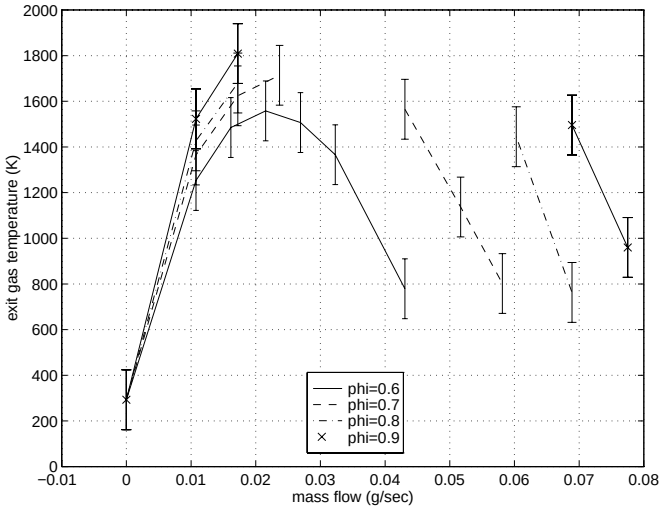

Fig. 19. Exit gas temperature measurements for ethylene-air combustion in the static structure. (Again, the break in the curve results from the inability to measure gas temperatures in excess of 1600K-1800K.)

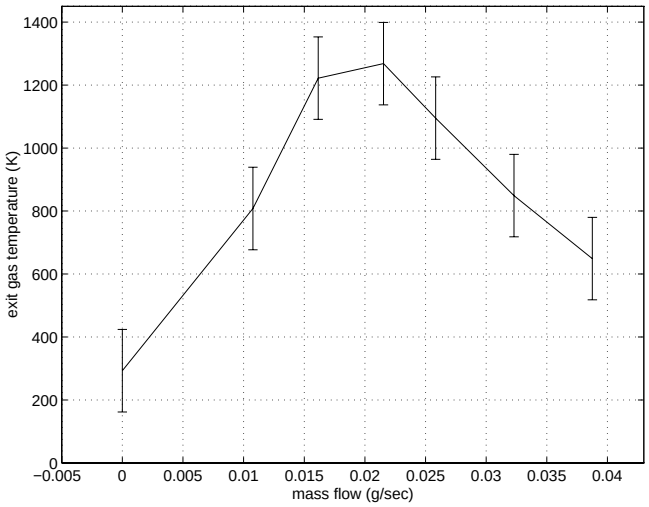

Fig. 20. Exit gas temperature measurements for propane-air combustion in the static structure (phi=0.8).

tween 60-80%, and a maximum power density of approximately 500 MW/m^3. Since the reaction rates for propane are much slower than those of ethylene, propane-air combustion could only be stabilized with power density levels of approximately 140 MW/m^3. For ethylene-air the minimum residence time for which stable combustion was obtained was $\approx$0.72 ms, whereas for propane-air it was $\approx$2.5 ms.

These results serve as the first experimental demonstration of stable hydrocarbon combustion within the structural constraints of a silicon chamber. Efforts are currently underway to further

examine the use of ethylene for a propulsion engine from a systems perspective, and to develop alternative catalytic strategies for design point hydrocarbon combustion in the microengine.

VII. Conclusions and Future Work

This paper presented the development of a 6-wafer combustion system for a silicon micro gas turbine engine. Fabricated by deep reactive ion etching through a total thickness of 3,800 μm, this structure serves as the first demonstration of the hot flow path of a multi-level microengine. The device was packaged with electrical and fluidic interconnects, and tested under hot-flow conditions in order to characterize its performance for hydrogen-air and hydrocarbon-air combustion. It survived high temperature operation for several tens of hours, thereby demonstrating the viability of silicon-based combustion systems for micro heat engine applications.

Future research work shall primarily focus on additional design point testing to establish combustion stability boundaries for the current design of the microengine, and to further develop hydrocarbon combustion strategies for the engine. The hot static components will also be integrated with the rotating compressor and turbine; first builds of the entire engine are expected in the year 2000.

Acknowledgments

The authors are grateful to Professor Alan H. Epstein for his direction throughout the course of this research, to Mr. Gregory Simpson at Thunderline-Z for his creative and enabling packaging solutions, and to Mr. Adam London, Mr. Todd Harrison and Professor Mark Spearing for their help with the process. We also acknowledge the technical support provided by Mr. Viktor Dubrowski and Mr. James LeTendre, and thank Ms. Lori Martinez, Ms. Diana Park and Ms. Holly Anderson for administrative help. We also thank all the other members of the MIT microengine team for their help and support, especially Dr. Chris Cadou, Dr. Eugene Huang, Mr. Steve Lukachko, Mr.

Jin-wook Lee and Ms. Sumita Pennathur.

This work was largely supported by ARO, Dr. R. Paur technical manager, and by DARPA, Dr. S. Wilson technical manager. All devices were fabricated at the MIT Microsystems Technology Laboratories; the support of the technical staff is gratefully acknowledged.

References

[1] Epstein *et al.*, *"Power MEMS and Microengines"*, presented at the IEEE Conference on Solid State Sensors and Actuators, Chicago, 1997.

[2] Epstein *et al.*, *"Micro-Heat Engines, Gas Turbines, and Rocket Engines"*, presented at the 28th AIAA Fluid Dynamics Conference and the 4th AIAA Shear Flow Control Conference, Snowmass Village, 1997.

[3] Groshenry, C., *"Preliminary Study of a Micro-Gas Turbine Engine"*, S.M. Thesis, Massachusetts Institute of Technology, 1995.

[4] Waitz *et al.*, *"Combustors for Micro-Gas Turbine Engines"*, ASME Journal of Fluids Engineering, Volume 120, March 1998.

[5] Mehra, A., Waitz, I. A., *"Development of a Hydrogen Combustor for a Microfabricated Gas Turbine Engine"*, presented at the Solid-State Sensor and Actuator Workshop at Hilton Head, 1998.

[6] Mehra *et al.*, *"Microfabrication of High Temperature Silicon Devices Using Wafer Bonding and Deep Reactive Ion Etching"*, to be published in the IEEE/ASME Journal of Microelectromechanical Systems, June 1999, Volume 8, Number 3.

[7] Chen, K-S., *"Materials Characterization and Structural Design of Ceramic Micro Turbomachinery"*, Ph.D. Thesis, Massachusetts Institute of Technology, 1999.

[8] Mehra, A., *"Development of a High Power Density Combustion System for a Silicon Micro Gas Turbine Engine"*, Ph.D. Thesis, Massachusetts Institute of Technology, 2000.

[9] Schetz, J. A., *"Injection and Mixing in Turbulent Flow"*, AIAA Prog. in Aeronautics and Astronautics, Vol. 68, 1980.

[10] Ayón *et al.*, *"Characterization of a Time Multiplexed Inductively Coupled Plasma Etcher"*, Journal of the Electrochemical Society, Vol. 146, No. 1, January 1999.

[11] Kern, W., Puotinen, D. A., "Cleaning Solutions Based on Hydrogen Peroxide for Use in Silicon Semiconductor Technology", RCA Review, Vol. 31, pp. 187-206, 1970.

[12] London, A. P., "Development and Test of a Microfabricated Bipropellant Rocket Engine", Ph.D. Thesis, Department of Aeronautics and Astronautics, Massachusetts Institute of Technology, (expected 2000).

[13] Coffee *et al.*, "The Overall Reaction Concept in Premixed, Laminar, Steady-State Flames. I. Stoichiometries", Combustion and Flame, 54: 155-169, 1983.

[14] Kuo, K. K., "Principles of Combustion", John Wiley & Sons, 1986.